Observer-based Control Design for Overhead Crane Systems

Kawai, Fukiko; Bendtsen, Jan D.

Published in:
IFAC-PapersOnLine

DOI (link to publication from Publisher):
10.1016/j.ifacol.2023.10.063

Publication date:
2023

Document Version
Publisher's PDF, also known as Version of record

Available online at www.sciencedirect.com

ScienceDirect

IFAC Papers Online CONFERENCE PAPER ARCHIVE

IFAC PapersOnLine 56-2 (2023) 8776–8783

Observer-based Control Design for Overhead Crane Systems

Fukiko Kawai * , **Jan D. Bendtsen** **

* *Fuji Electric Co., Ltd., Tokyo, Japan. (e-mail: kawai-fukiko@fujielectric.com)*

** *Aalborg University, 9220 Aalborg, Denmark (e-mail: dimon@es.aau.dk)*

Abstract: This paper proposes an observer-based control design with Disturbance Feedback Control (DFC) for overhead crane systems. DFC is a technique to improve the disturbance rejection capabilities of existing control loops. The crane system is modelled with 3D dynamics and linearized. Payload sway angles are estimated by a Kalman Filter. A state feedback controller for setpoint tracking and a DFC for disturbance rejection are designed using Linear Matrix Inequalities. Both simulation and experimental results show that the observer-based control with DFC can estimate the sway angle and is able to attenuate disturbance inputs better than the conventional observer-based control. The proposed design can thus achieve practical angle sensor-less control with a retro-fit modification of an existing control.

Keywords: Crane systems, Anti-Sway Control, Kalman Filter, Robust Control

1. INTRODUCTION

State-of-the-art crane control systems of today are supplied with anti-sway crane control embedded in speed drives (inverters) and Programmable Logic Controllers (PLCs) to yield both high performance and usability. However, such systems are expensive and, like many other advanced manufacturing industries, crane control manufacturers must find ways to 'achieve more with less.' *Sensorless* systems is one example of providing important added-value to lower-end crane systems due to compactness and lower cost, both in case of new and retrofitted crane systems. However, the control scheme must of course remain able to estimate the sway angle of the payload, while at the same time maintaining robustness against disturbances such as wind and (small) collisions without being able to rely on measurements of the sway angles.

In this paper a sensorless add-on control configuration for a generic overhead crane control system, known as Disturbance Feedback Control (DFC), is discussed. This control structure utilizes an additional feedback to compensate for disturbance and model uncertainties, but otherwise maintains the existing control system as is. From a practitioner's point of view this step-wise approach is advantageous, since it allows tuning the guiding controller using standard techniques first, and then adding the disturbance attenuation feedback later, for instance as a retrofit option.

In a previous study, Kawai et al. (2018), the authors proposed a robust DFC scheme for 2D Gantry cranes for shipping applications. Several stability conditions that the DFC law must satisfy in order to guarantee stable closed-loop operation were subsequently formulated in Bendtsen and Kawai (2019). In particular, it was found that the nominal model of the system must be *open-loop stable* for the scheme to have any chance of guaranteeing internal stability in the face of exogenous disturbances. However, these results assumed full state feedback; for sensorless control, it is necessary to consider state estimation as well.

Several results on observer-based control for crane systems have been published in the literature. An Unscented Kalman filter was designed to estimate the states of the motion of the load in Kreuzer et al. (2014). The observer was validated in a container crane test stand. For disturbance estimation, finite-time disturbance observers were proposed to estimate external disturbances in Jin-Hua She et al. (2004) and Zhang et al. (2018).

Other results on soft sensor-based control for crane applications have been presented as alternatives to observer-based control. For example, a scheme based on artificial neural networks was proposed in Solihin et al. (2006), while a soft sensor to estimate the sway angle using dual microphones was proposed in Nakamoto et al. (2020).

Other control designs for crane systems have focused on robustness as well; for instance, an optimal robust controller was designed based on μ-synthesis and DK-iteration in Moradi and Vossoughi (2015). However, the authors have not been able to find any combinations of robust design with retro-fit modification and sensorless crane control in the literature so far.

In preparation for future implementation on actual overhead crane systems, this paper proposes a novel robust anti-sway DFC scheme based on Linear Matrix Inequality-based (LMI) optimization. A model-based soft sensor provides a full state estimate based on trolley position and speed measurements only, which are readily available in standard overhead crane systems, and employs this full-state estimate for the additive DFC feedback. Both set point regulation and disturbance rejection responses are examined with and without robust DFC through simula-

10.1016/j.ifacol.2023.10.063

tions on a non-linear model as well as through laboratory tests. Noticeable disturbance rejection performance improvements are observed, with no impact on the reference following capabilities of the existing controller.

The outline of the rest of the paper is as follows. Section 2 first briefly presents the 3D crane model used for simulation along with a linearized version used for conventional design. Subsequently, an Extended Kalman Filter for the proposed DFC is introduced in Section 3. Next, Section 4 formulates the robust design problem and the LMIs used to solve it. After that, numerical examples are presented in Section 5 and Experimental test in Section 6 are demonstrated. Finally, conclusions are given in Section 7.

2. 3D MODELING OF OVERHEAD CRANE SYSTEMS

2.1 Crane System Model

Fig. 1 shows the 3D crane model considered in this work; it was originally derived in Kaneshige et al. (1998). The model complexity is chosen as a trade-off between accuracy and feasibility of control design for fast control systems; more complex mathematical models than presented here can certainly be derived, but too complex designs cannot be implemented in industry-standard control devices such as PLCs, operating with control cycle times on the order of milliseconds with computational resources.

The motion of the trolley is given by the following (scalar [1]) linear differential equations:

$$\ddot{x} = -\frac{1}{T_x}\dot{x} + \frac{K_x}{T_x}u_x \tag{1}$$

$$\ddot{y} = -\frac{1}{T_y}\dot{y} + \frac{K_y}{T_y}u_y \tag{2}$$

$$\ddot{z} = -\frac{1}{T_z}\dot{z} + \frac{K_z}{T_z}u_z \tag{3}$$

where $x = x(t)$, $y = y(t)$ are the coordinates of the position of the trolley at time $t \geq 0$, $z = z(t)$ is the cable extension length at time t, T_x, T_y, T_z, K_x, K_y, and K_z are motor time constants and gains, respectively, and $u_x = u_x(t)$, $u_y = u_y(t)$ and $u_z = u_z(t)$ are the speed command signals of each axis.

The coordinates of the payload position $(\tilde{x}(t),\ \tilde{y}(t),\ \tilde{z}(t))$ are given by

$$\tilde{x} = x + z\sin\theta\cos\varphi \tag{4}$$

$$\tilde{y} = y + z\sin\theta\sin\varphi \tag{5}$$

$$\tilde{z} = z\cos\theta \tag{6}$$

where $\theta = \theta(t)$ and $\varphi = \varphi(t)$ are defined as shown in Fig. 1.

The equations of motion for the payload in the vicinity of its equilibrium can be derived from Newton's second law applied along each coordinate axis:

[1] We generally consider real scalar signals by default throughout the paper and provide dimensions of vectors and matrices unless these are obvious from the context. We use the notation n_ψ to indicate the dimension of any vector ψ.

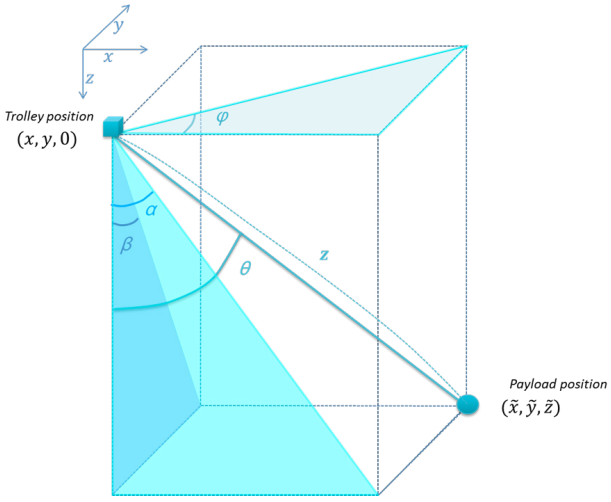

Fig. 1. Sketch of crane model for control design.

$$m\ddot{\tilde{x}} = -F\sin\theta\cos\varphi - D_\alpha(\dot{\tilde{x}} - \dot{x}) \tag{7}$$

$$m\ddot{\tilde{y}} = -F\sin\theta\sin\varphi - D_\beta(\dot{\tilde{y}} - \dot{y}) \tag{8}$$

$$m\ddot{\tilde{z}} = mg - F\cos\theta \tag{9}$$

where m is the mass of the payload, F is the cable tension due to the payload suspension, and D_α and D_β are damping coefficients.

Combining Equations (4)–(9) thus yields the following model:

$$m\ddot{\tilde{x}} = -F\frac{\tilde{x} - x}{z} - D_\alpha(\dot{\tilde{x}} - \dot{x}) \tag{10}$$

$$m\ddot{\tilde{y}} = -F\frac{\tilde{y} - y}{z} - D_\beta(\dot{\tilde{y}} - \dot{y}) \tag{11}$$

$$m\ddot{\tilde{z}} = mg - F\frac{\tilde{z}}{z} \tag{12}$$

and the sway angle of the payload is given by

$$\alpha = \tan^{-1}\frac{\tilde{x} - x}{\tilde{x}}, \quad \beta = \tan^{-1}\frac{\tilde{y} - y}{\tilde{y}} \tag{13}$$

where α and β are projection angles (again, see Fig. 1).

2.2 Crane Model for Control Design

The model above is linearized in an operating point; $\theta = \varphi = 0$ is chosen for both the conventional design and the subsequent LMI-based design, resulting in the quasi-Linear Parameter Varying (quasi-LPV) model

$$\dot{\xi} = A(z)\xi + B_2 u, \tag{14}$$

where $\xi = [x,\ \dot{x},\ \Delta x,\ \Delta\dot{x},\ y,\ \dot{y},\ \Delta y,\ \Delta\dot{y},\ z,\ \dot{z}]^{\mathrm{T}}$ is the state vector, $\Delta x = \tilde{x} - x$, $\Delta y = \tilde{y} - y$, $\Delta z = \tilde{z} - z$, $u = [u_x,\ u_y,\ u_z]^{\mathrm{T}}$, and

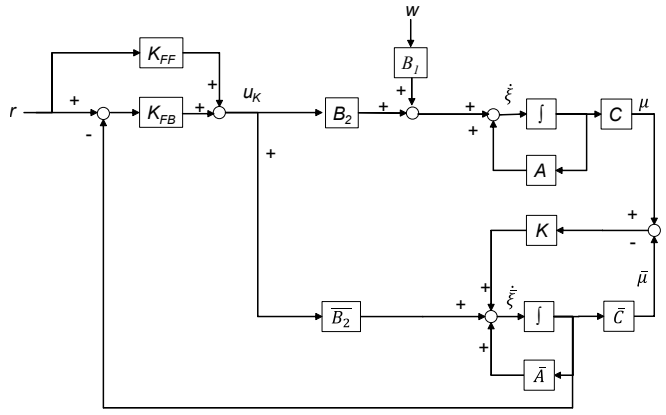

Fig. 2. Block diagram of an existing crane control system with Kalman Filter (continuous time).

$$A(z) = \begin{bmatrix} 0 & 1 & 0 & 0 & 0 & 0 & 0 & 0 & 0 & 0 \\ 0 & \frac{-1}{T_x} & 0 & 0 & 0 & 0 & 0 & 0 & 0 & 0 \\ 0 & 0 & 0 & 1 & 0 & 0 & 0 & 0 & 0 & 0 \\ 0 & \frac{1}{T_x} & \frac{-g}{z} & \frac{-D_\alpha}{m} & 0 & 0 & 0 & 0 & 0 & 0 \\ 0 & 0 & 0 & 0 & 0 & 1 & 0 & 0 & 0 & 0 \\ 0 & 0 & 0 & 0 & 0 & \frac{-1}{T_y} & 0 & 0 & 0 & 0 \\ 0 & 0 & 0 & 0 & 0 & 0 & 0 & 1 & 0 & 0 \\ 0 & 0 & 0 & 0 & 0 & \frac{1}{T_y} & \frac{-g}{z} & \frac{-D_\beta}{m} & 0 & 0 \\ 0 & 0 & 0 & 0 & 0 & 0 & 0 & 0 & 0 & 1 \\ 0 & 0 & 0 & 0 & 0 & 0 & 0 & 0 & 0 & \frac{-1}{T_z} \end{bmatrix},$$

$$B_2 = \begin{bmatrix} 0 & \frac{K_x}{T_x} & 0 & \frac{-K_x}{T_x} & 0 & 0 & 0 & 0 & 0 & 0 \\ 0 & 0 & 0 & 0 & 0 & \frac{K_y}{T_y} & 0 & \frac{-K_y}{T_y} & 0 & 0 \\ 0 & 0 & 0 & 0 & 0 & 0 & 0 & 0 & 0 & \frac{K_z}{T_z} \end{bmatrix}^{\mathrm{T}}$$

are the state and input matrices, respectively.

Note that z appears in the matrix A, which means that (14) is in fact nonlinear; however, inspired by real-world crane operation it is assumed to remain constant during operation in the (x, y) plane (when the load is in transit toward its destination), permitting us to consider it as a parameter in a quasi-LPV setting. This assumption is purely for convenience, however, since the design is deliberately made robust to bounded variations in z.

3. KALMAN ESTIMATOR

This section describes the Kalman estimator introduced in the existing control system and the control system augmented with DFC for estimating the sway width of the pay load. The design is mostly standard; see e.g. Särkkä (2013) for a more thorough presentation of Kalman estimator/filter theory. Block diagrams depicting observer based control with KF and with/without DFC are shown in Figs. 2 and 3, respectively. Note that $\mu = [x,\ \dot{x},\ y,\ \dot{y},\ z,\ \dot{z}]^{\mathrm{T}}$ is a measurement vector of the trolley position and velocity in 3 dimensions.

Discretizing the crane system model above with a fixed sample rate and introducing Gaussian noise on states and measurements results in

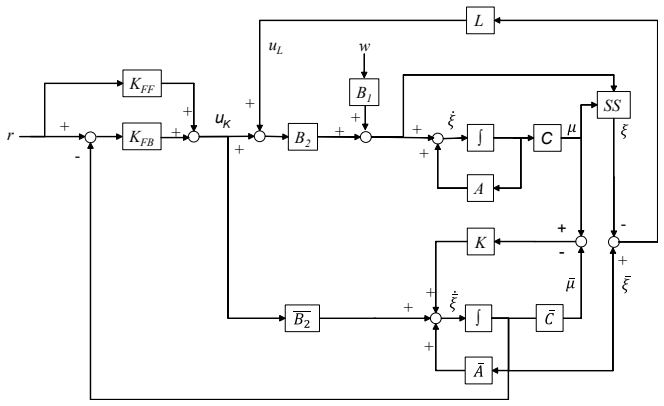

Fig. 3. Block diagram of an existing crane control system which is augmented with both Disturbance Feedback Control and Kalman Filter (continuous time).

$$\begin{aligned} \xi_k &= \Phi\xi_{k-1} + \Gamma u_k + w_k \\ \mu_k &= C\xi_k + v_k \end{aligned} \tag{15}$$

where $\Phi \in \mathbb{R}^{n_\xi \times n_\xi}$, $\Gamma \in \mathbb{R}^{n_\xi \times n_u}$ are discretized state, input, and noise gain matrices, $w_k \sim \mathcal{N}(0,\, Q)$ is process noise, and $v_k \sim \mathcal{N}(0,\, R)$ is measurement noise, all at time step k.

A Kalman filter gain $K_k \in \mathbb{R}^{n_\xi \times n_\mu}$ can then be introduced and tuned using the well-known Kalman Filter algorithm. First the prediction step:

$$\begin{aligned} \hat{\xi}_k^- &= \Phi\hat{\xi}_{k-1}^- + \Gamma u_k \\ P_k^- &= \Phi P_{k-1}^- \Phi^{\mathrm{T}} + Q_{k-1} \end{aligned} \tag{16}$$

where $\hat{\xi}_k^-$ is the state estimate at time step k, and P_k^- is the predicted covariance estimate at the time step k just before the measurement y. Note that superscript $(^-)$ means that states and matrices are evaluated at the prediction step.

Next, the Kalman gain K_k, state estimate $\hat{\xi}_k$, and covariance matrix P_k are updated in a correction step:

$$K_k = P_k^- C^T (C P_k^- C^T + R)^{-1} \tag{17}$$

$$\hat{\xi}_k = \hat{\xi}_k^- + K_k(\mu_k - C\xi_k^-) \tag{18}$$

$$P_k = (I - K_k C) P_k^-. \tag{19}$$

4. DISTURBANCE FEEDBACK CONTROL DESIGN

This section describes a robust DFC design method by using LMI optimization. The DFC design in this work is taken from Kawai et al. (2018).

4.1 Control configuration

Fig. 3 shows the closed-loop system with DFC (in continuous time), where r is the reference input, $u = u_{\mathrm{K}} + u_{\mathrm{L}}$ is the control input, w is the disturbance, B_1 is a gain matrix for w, and A and B_2 are plant model matrices (given above, with z assumed fixed). The existing controller is specified by a feedforward term K_{FF} and a feedback term K_{FB}. The DFC comprises a nominal plant model specified by nominal parameter matrices $\bar{A}$ and $\bar{B}_2$ along with the disturbance feedback L. The true states of the plant are denoted ξ, while $\bar{\xi}$ contains the states of the nominal plant model. Note that the observer-based control cannot access the sway width information in the state vector ξ of the

real plant. An online simulator is therefore implemented in order to compute $\Delta x,\ \Delta\dot{x},\ \Delta y,\ \Delta\dot{y}$ in the soft sensor (SS) block to replace real sensor measurements.

The DFC then makes use of the error between real measurements and the Kalman filter state estimate. Here, we make use of the soft sensor measurements from the SS block to provide the missing measurements for constructing the error signal for the DFC.

As noted in the Introduction we stipulate that K_{FF} and K_{FB} remain fixed; thus, the existing controllers are considered part of the plant in the following robust DFC design setup.

4.2 Parametric Uncertainty Model

Parametric uncertainties in the crane system model must be considered in order to achieve a robust design. Let the true plant be

$$\dot{\xi} = A\xi + B_2 u, \tag{20}$$

with the plant parameters being affected by polytopic uncertainties

$$A = \bar{A} + \sum_{i=1}^{q} \delta_{a,i} A_i, \quad \delta_{a,i} \in [-1, 1]. \tag{21}$$

Here, $(\delta_{a,1}, \ldots, \delta_{a,q})$ are unknown constants multiplied by known (also constant) matrices A_i, see e.g. Carsten Scherer and Siep Weiland (2004). The design has to guarantee both stability and performance for all possible values of the unknown parameters $\delta_{a,i}$. [2]

4.3 State Feedback Control (Existing Controller)

The state feedback controller is given as existing controller.

$$u_{\mathrm{K}} = K_{\mathrm{FB}} e, \tag{22}$$

where $K_{\mathrm{FB}} \in \mathbb{R}^{n_u \times n_\xi}$ is a state feedback gain and $e = r - \bar{\xi}$, and

$$\bar{\xi} = \begin{bmatrix} \bar{x} & \dot{\bar{x}} & \Delta\bar{x} & \Delta\dot{\bar{x}} & \bar{y} & \dot{\bar{y}} & \Delta\bar{y} & \Delta\dot{\bar{y}} & \bar{z} & \dot{\bar{z}} \end{bmatrix}^{\mathrm{T}}$$

is the state vector of the nominal plant model.

4.4 Robust DFC Design

The DFC is chosen as

$$u_{\mathrm{L}} = L\epsilon, \tag{23}$$

where $L \in \mathbb{R}^{n_u \times n_\xi}$ is the disturbance feedback gains, $\epsilon = \bar{\xi} - \xi$.

The extended state space representation of the overall system at the extremal values of the uncertainties can then be described as follows:

$$\dot{\chi} = A_{\mathrm{aug},\delta}\chi + B_{\mathrm{aug},1} w + B_{\mathrm{aug},2} u_l \tag{24}$$

where

$$\chi = \begin{bmatrix} \xi \\ \bar{\xi} \end{bmatrix}, \quad A_{\mathrm{aug},\delta} = \begin{bmatrix} A_\delta - B_2 K_{FB} & 0 \\ -\bar{B}_2 K_{FB} & \bar{A} \end{bmatrix},$$
$$B_{\mathrm{aug},1} = \begin{bmatrix} B_1 \\ 0 \end{bmatrix}, \quad B_{\mathrm{aug},2} = \begin{bmatrix} B_2 \\ 0 \end{bmatrix},$$

and w is an input disturbance, the A_δ is any extremal value of A as stated in (21).

[2] Note that z is considered the primary uncertain parameter here, but the framework allows easy incorporation of other uncertain parameters such as the payload mass m as well.

Extremal values of the uncertain closed loop transfer function T from w to χ is then computed as follows:

$$\dot{\chi} = \mathcal{A}_\delta \chi + \mathcal{B} w \tag{25}$$

where

$$(\,\mathcal{A}_\delta \,|\, \mathcal{B}\,) = \left(\begin{array}{cc|c} A_\delta - B_2 K_{FB} - B_2 L & B_2 L & B_1 \\ -B_2 K_{FB} & \bar{A} & 0 \end{array} \right). \tag{26}$$

The robust DFC design is now formulated by using the dominant region (Boyd et al. (1994)):

$$\begin{aligned} & 2\alpha\mathcal{X} + {\mathcal{A}_\delta}^{\mathrm{T}}\mathcal{X} + \mathcal{X}\mathcal{A}_\delta < 0, \\ & \mathcal{X} = \begin{bmatrix} X_1 & X_0 \\ X_0 & X_2 \end{bmatrix}, \quad \mathcal{X} > 0, \\ & X_0 > 0. \quad X_1 > 0, \quad X_2 > 0, \end{aligned} \tag{27}$$

where

$$\begin{aligned} \mathcal{A}_\delta \mathcal{X} &= \begin{bmatrix} A_\delta - B_2 K_{FB} - B_2 L & B_2 L \\ -B_2 K_{FB} & \bar{A} \end{bmatrix} \begin{bmatrix} X_1 & X_0 \\ X_0 & X_2 \end{bmatrix} \\ &= \begin{bmatrix} \mathcal{A}_\delta \mathcal{X}_{1,1} & \mathcal{A}_\delta \mathcal{X}_{1,2} \\ \mathcal{A}_\delta \mathcal{X}_{2,1} & \mathcal{A}_\delta \mathcal{X}_{2,2} \end{bmatrix} \end{aligned}$$

$\mathcal{A}_\delta \mathcal{X}_{1,1} = (A_\delta - B_2 K_{FB}) X_1 + B_2(-Y + V)$,
$\mathcal{A}_\delta \mathcal{X}_{1,2} = (A_\delta - B_2 K_{FB}) X_0 + B_2(-V + W)$,
$\mathcal{A}_\delta \mathcal{X}_{2,1} = -B_2 K_{FB} X_1 + \bar{A} X_0$,
$\mathcal{A}_\delta \mathcal{X}_{2,2} = -B_2 K_{FB} X_0 + \bar{A} X_2$,
$V := LX_0$, $Y := LX_1, W := LX_2$. The subscript-δ notation should be understood as requiring the LMIs to be satisfied for all extremal points of δ_a as defined in (21). That is, the LMIs must be satisfied everywhere on the convex hull defined by the permissible values of the uncertainties, implying that one LMIs has to be solved for every vertex of the hypercube $\delta_a \in [-1, 1]^q$ in order to yield one common $\mathcal{X}$. When the LMIs are solved, the DFC gain L may be found as three different solutions from V, Y, and W, respectively; either may be chosen, as long as the DFC stabilizes the closed loop system.

5. SIMULATION EXAMPLES

This section demonstrates simulation examples for evaluating the observer based DFC. First, a state feedback control K_{FB} and a DFC L are designed assuming full state measurements are available, and the poles and zeros are examined to confirm nominal stability (cf. Bendtsen and Kawai (2019)). After that, observer-based control designs with and without DFC are examined in time-domain simulation. The simulation examples are carried out with nominal model in rope length $l = 0.9$ m, and the rope length is varying from 0.9 to 0.8 m in Table 2. The plant and KF model are discretized by the Forward Euler method with a sampling interval of 5 ms (a common option for standard PLCs), while the nominal model is simulated using 4th order Runge-Kutta integration in Matlab. The simulations are evaluated in terms of robustness against impulse disturbances along the x- and y-axis.

5.1 Model parameters

Table 1 lists parameter values of the crane system model.

Table 2. Simulation conditions.

Item	Value	Unit
Control cycle in Matlab	5×10^{-3}	s
Data sampling time	5×10^{-3}	s
Set point of trolley in x- axis	0.8	m
Set point of trolley in y- axis	0.8	m
Set point of rope length in z- axis	0.8	m
Upper limit of trolley velocity	0.3	m/s
Simulation time	60	s
Time of impulse disturbance in x- axis	25	s
Time of impulse disturbance in y- axis	30	s
Pulse width of disturbance	1	s
Pulse amplitude of disturbance	0.1 $\times 10^5$	N

Table 1. Parameter values of the crane system model.

Parameter	Value	Unit
m	0.5	kg
K_x	1.0	-
K_y	1.0	-
K_z	1.0	-
T_x	0.11	sec
T_y	0.10	sec
T_z	0.05	sec
D_α	0.0264	-
D_β	0.0264	-
l	[0.8, 1.0]	m
g	9.8	m/s^2

5.2 Evaluations of DFC design

The DFC gain matrix L is found by solving the LMI problem (27) using YALMIP and SDP solver SeDuMi-1.3 for Matlab (see Löfberg (2004)).

The Kalman gain was found to converge in about 10 time steps (corresponding to 0.05 seconds), indicating that it is likely appropriate to simply use a constant Kalman gain to estimate the states in most real-life crane system.

The converged Kalman gain is applied to both a simulation test in next subsection, and a realistic laboratory test in section 6.

5.3 Simulation Results

Table 2 shows simulation conditions for the time-domain simulation. 3D tracking control is examined for 25 seconds, and then an input disturbance is added to both the x- and y-axis in order to evaluate disturbance rejection. Fig. 4 shows simulation results of observer-based control with and without DFC. Payload position estimates along the x- and y-axes are plotted in the third and 7th subfigures, respectively. The observer-based control with constant Kalman gain are found to be able to estimate the main dynamics of the sway in payload in the tracking control.

As can be seen from the responses after the disturbances are introduced at $t = 25$ seconds, the observer-based control without DFC performs considerably poorer in terms of both payload estimation and anti-sway control performance. On the other hand, it is seen that the observer-based control with DFC is able to improve the disturbance attenuation after input pulse disturbances along both x- and y-axes.

Table 3. Maximum and minimum sway width of the disturbance responses in Matlab simulation.

Sway width	Conventional method ($K_{\mathrm{FF}} + K_{\mathrm{FB}}$) [mm]	Proposed method ($K_{\mathrm{FF}} + K_{\mathrm{FB}}$ $+DFC$) [mm]
Max. along x- axis	63.6	32.8
Min. along x- axis	-63.8	-21.2
Max. along y- axis	65.0	32.4
Min. along y- axis	-65.2	-21.0

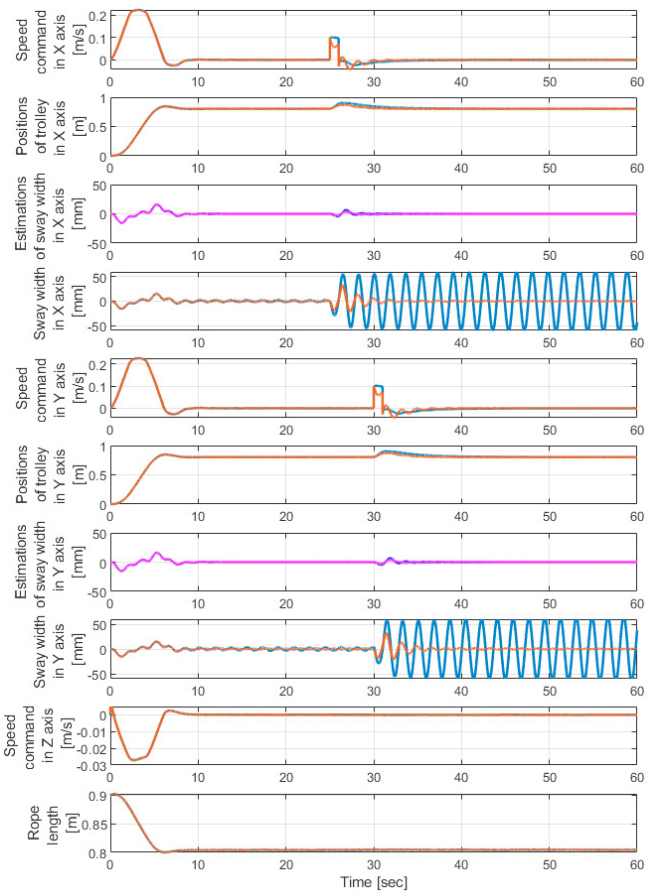

Fig. 4. Simulation results of observer based control with DFC in orange line, without DFC in blue line.

Table 3 lists various key values obtained in the simulation of the disturbance responses. The proposed method improved the maximum and minimum load deviation along the x-axis by 30.8 and 42.8 mm, respectively, while for the y-axis load deviation the improvement was 32.6 and 44.2 mm, respectively; a considerable improvement in both cases. It is thus concluded that the sensorless anti-sway control works as intended, and that DFC improves (impulse) disturbance rejection.

Fig. 5 shows simulation results of state feedback control with and without DFC. Both control schemes are able to attenuate the effects of the input disturbances and make the sway width converge to 0. However, as shown in Fig. 4, the observer-based control without DFC has considerably poorer disturbance rejection disturbance.

The simulation results thus indicate that DFC yields the same control performance, regardless of whether it is used

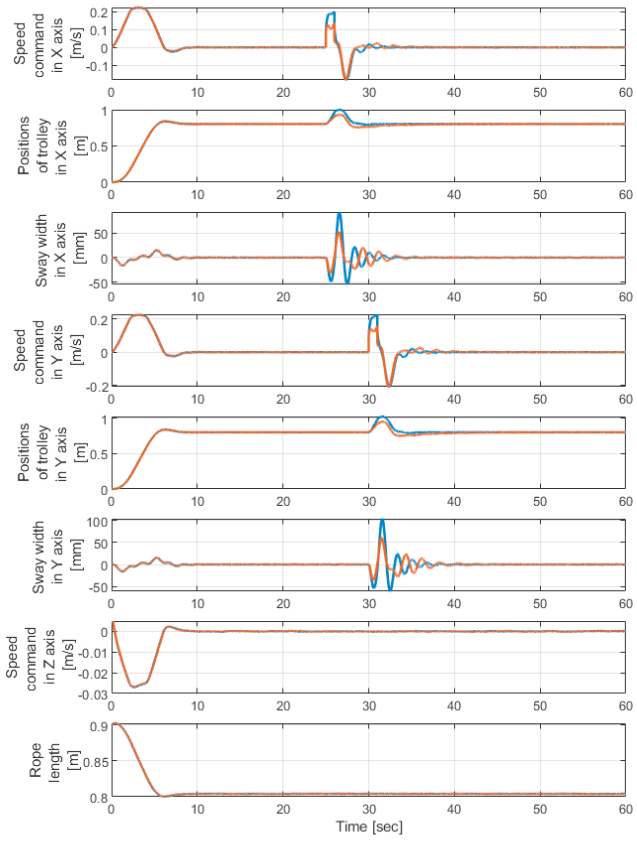

Fig. 5. Simulation results of state feedback control with DFC in orange line, without DFC in blue line.

with observer-based control or state feedback control. It is furthermore confirmed that the sensorless control method does not exhibit performance deterioration.

6. EXPERIMENTAL RESULTS

This section shows experimental verification of the observer-based control with and without DFC on an overhead crane laboratory setup.

6.1 Experimental Setup

The laboratory test setup in Fig. 6 is a scaled-down version of a realistic overhead crane system. The system parameters of the crane model is the same as simulation condition in Table 1. The test conditions in Table 4 are designed based on the simulation results in section 5. Note that the Kalman gain is kept constant in the laboratory test, since the update algorithm requires a matrix inverse calculation, and this calculation is too heavy to implement on the PLC used in the test setup. The constant Kalman gain is chosen as the value of K 30 seconds into the simulation with tracking and disturbance responses.

6.2 Test Results

Fig. 7 shows experimental results of observer-based control with and without DFC. Payload position estimates

Table 4. Test conditions.

Item	Value	Unit
Control cycle in PLC	5×10^{-3}	s
Data sampling time	1×10^{-1}	s
Set point of trolley in x- axis	0.8	m
Set point of trolley in y- axis	0.8	m
Set point of rope length in z- axis	0.8	m
Upper limit of trolley velocity	0.2	m/s
Test time	60	s
Time of impulse disturbance in x- axis	25	s
Time of impulse disturbance in y- axis	30	s
Pulse width of disturbance	1	s
Pulse amplitude of disturbance	0.1×10^5	N

Table 5. Maximum and minimum sway width of the disturbance responses in experimental results.

Sway width	Conventional method ($K_{\mathrm{FF}} + K_{\mathrm{FB}}$) [mm]	Proposed method ($K_{\mathrm{FF}} + K_{\mathrm{FB}}$ $+DFC$) [mm]
Max. along x- axis	36.53	16.79
Min. along x- axis	-27.78	-13.19
Max. along y- axis	45.90	26.88
Min. along y- axis	-47.84	-21.93

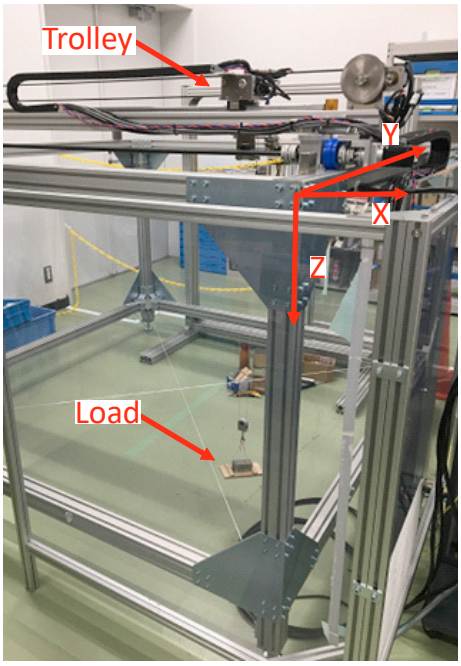

Fig. 6. Overhead crane systems setup.

along the x- and y-axes are plotted in the third and 7th subfigures, respectively. The observer-based control with constant Kalman gain are found to be able to estimate the main dynamics of the sway in payload in the tracking control. As can be seen from the responses after the disturbances are introduced at $t = 25$ seconds, the observer-based control without DFC performs considerably poorer in terms of both payload estimation and anti-sway control performance. On the other hand, it is seen that the observer-based control with DFC is able to improve the disturbance attenuation after input pulse disturbances along both x- and y-axes.

Table 5 lists various key values obtained in the simulation of the disturbance responses. The proposed method im-

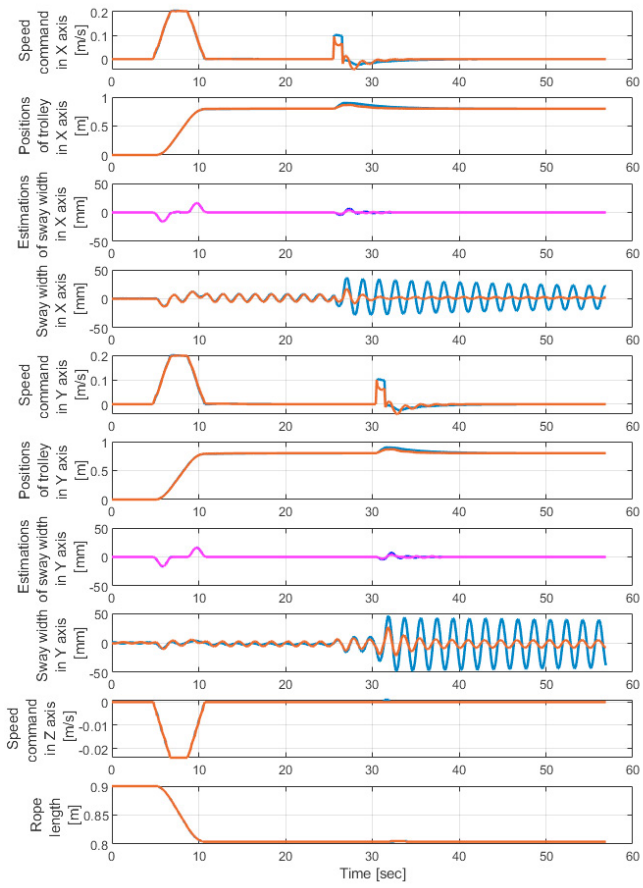

Fig. 7. Experimental results of observer based control with DFC in orange line, without DFC in blue line.

proved the maximum and minimum load deviation along the x-axis by 19.74 and 14.59 mm, respectively, and by 19.03 and 25.91 mm along the y-axis, respectively. It is thus concluded that the sensorless anti-sway control works as intended, and that DFC improves (impulse) disturbance rejection.

2D plots of the trolley positions and 3D plots of the payload positions with and without DFC are shown in Fig. 8. It is seen that both control schemes are eventually able to position the payload at the target position (indicated by a red square marker □), but the DFC scheme uses the trolley more actively to attenuate the oscillations in the payload.

On a side note, it is observed in the laboratory tests that the proposed method with DFC tends to attenuate *rotation* of the payload as well, which although not technically a part of the design, certainly is a desirable feature in shipping applications.

7. CONCLUSION

This paper proposes an observer based control scheme with Disturbance Feedback Control (DFC) for overhead crane systems. The crane system is modelled with 3D dynamics and linearized to obtain a quasi-LPV system. Sway angles of pay load are estimated by a Kalman Filter. The control gains are designed using an LMI-based approach to achieve robustness toward known parameter variations, most notably the rope length. Simulation results show that observer based control with DFC can estimate the sway angle and improve disturbance rejection compared to the baseline design, conventional observer based control design. The design was further verified on a laboratory-scale overhead crane setup under more realistic circumstances, such as implementation on industry-standard PLCs etc.

Future work will consider the stability conditions of the proposed method with Kalman state estimation, as well as LPV-style designs that can incorporate the rope length directly in the DFC design.

REFERENCES

Jan Bendtsen and Fukiko Kawai. Internal stability of disturbance feedback control loops. In *Proc. IEEE Conference on Control Technology and Applications*, pages 450–455, Hong Kong, 2019.

S. Boyd, L. EI Ghaoui, E. Feron, and V. Balakrishnan. *Linear Matrix Inequalities in System and Control Theory*. Volume 15 of Studies in Applied Mathematics, Society for Industrial and Applied Mathematics (SIAM)., Philadelphia, USA, 1994.

Carsten Scherer and Siep Weiland. Linear matrix inequalities in control, 2004. URL `http://www.dcsc.tudelft.nl/~cscherer/lmi/notes05.pdf`.

Jin-Hua She, H. Kobayashi, Y. Ohyama, and Xin Xin. Disturbance estimation and rejection - an equivalent input disturbance estimator approach. In *2004 43rd IEEE Conference on Decision and Control (CDC) (IEEE Cat. No.04CH37601)*, volume 2, pages 1736–1741 Vol.2, Dec 2004. doi: 10.1109/CDC.2004.1430295.

A. Kaneshige, Kazuhiko Terashima, and takeshi Sadamori. Modeling and transferring control of an overhead traveling crane based on the information of object position. *Trans. Japan Soc. Mech. Engineers, Series C*, 64(628): 4777–4782, 1998. doi: 10.1299/kikaic.64.4777.

Fukiko Kawai, Takashi Hayashi, Takayuki Kaneko, Palle Andersen, and Jan Bendtsen. Anti-sway control for crane systems: Robust design with LMI optimization. In *Proc. IEEE Conference on Control Technology and Applications*, pages 716–721, Copenhagen, 2018.

Edwin Kreuzer, Marc-André Pick, Christian Rapp, and Julian Theis. Unscented Kalman Filter for Real-Time Load Swing Estimation of Container Cranes Using Rope Forces. *Journal of Dynamic Systems, Measurement, and Control*, 136(4), 04 2014. ISSN 0022-0434. doi: 10.1115/1.4026602. URL `https://doi.org/10.1115/1.4026602`. 041009.

J. Löfberg. Yalmip : A toolbox for modeling and optimization in matlab. In *In Proceedings of the CACSD Conference*, Taipei, Taiwan, 2004.

Hamed Moradi and Gholamreza Vossoughi. State estimation, positioning and anti-swing robust control of traveling crane-lifter system. *Applied Mathematical Modellingl*, 39(22):6990–7007, 2015.

Masayoshi Nakamoto, Hanako Ogawa, and Naoki Horie. Soft sensor for sway angle of overhead crane using phase difference of acoustic signals. In *IECON 2020 The 46th Annual Conference of the IEEE Industrial Electronics Society*, pages 736–741, 2020. doi: 10.1109/IECON43393.2020.9254530.

Simo Särkkä. *Bayesian Filtering and Smoothing*. Cambridge University Press., Cambridge, 2013.

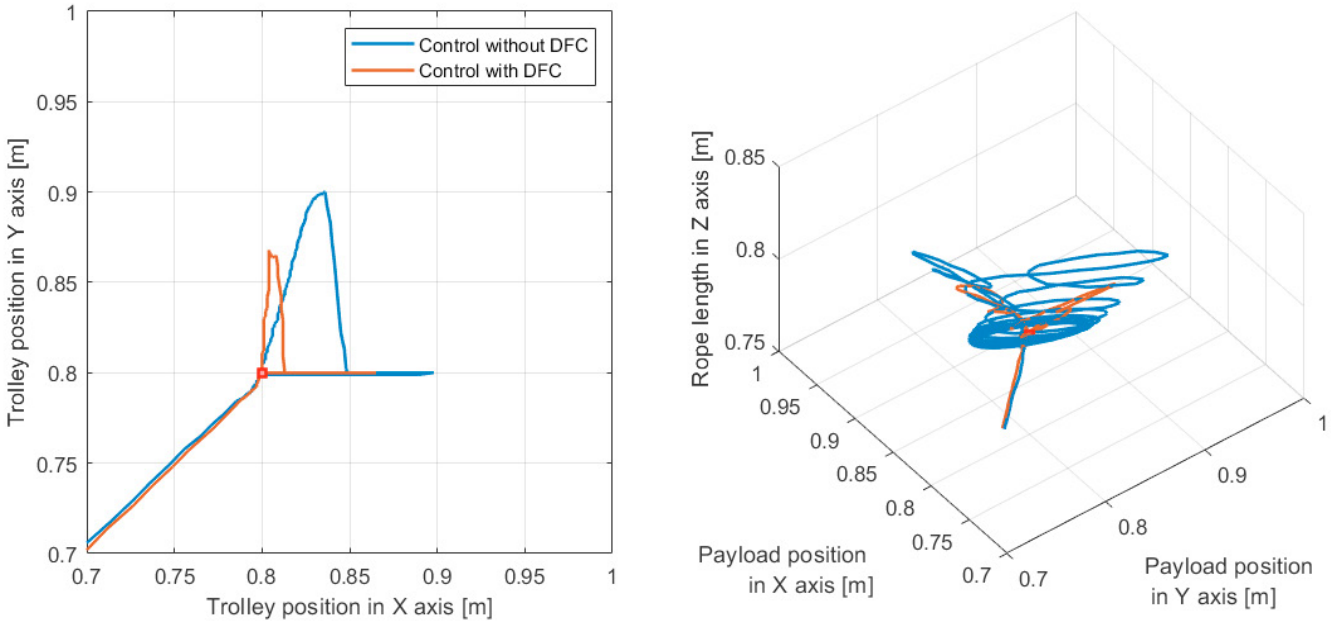

Fig. 8. 2D plot of trolley positions (left) and 3D plot of payload positions (right); with DFC in blue, without DFC in orange, set point in square marker (□).

Mahmud Iwan Solihin, Wahyudi, and Abdulgani Albagul. Development of soft sensor for sensorless automatic gantry crane using rbf neural networks. In *2006 IEEE Conference on Cybernetics and Intelligent Systems*, pages 1–6, 2006. doi: 10.1109/ICCIS.2006.252278.

Z. Zhang, L. Li, and Y. Wu. Disturbance-observer-based antiswing control of underactuated crane systems via terminal sliding mode. *IET Control Theory Applications*, 12(18):2588–2594, 2018. doi: 10.1049/iet-cta.2018.5344.